

---

# Carbonization of Zr-Loaded Thiourea-Functionalized Styrene-Divinylbenzene Copolymers: An Easy Way to Synthesize Nano-ZrO<sub>2</sub>@C and Nano-(ZrC, ZrO<sub>2</sub>)@C Composites

---

[Alejandro Martiz](#) , [Zoltán Károly](#) , [Laura Bereczki](#) , [László Trif](#) , [Attila Farkas](#) , Alfréd Menyhárd , [László Kótai](#) \*

Posted Date: 30 June 2023

doi: 10.20944/preprints202306.2203.v1

Keywords: zirconium carbide; zirconium dioxide; carbon matrix; graphite; RF plasma; carbonization; thiourea; styrene-divinylbenzene copolymer; Raman spectroscopy



Preprints.org is a free multidiscipline platform providing preprint service that is dedicated to making early versions of research outputs permanently available and citable. Preprints posted at Preprints.org appear in Web of Science, Crossref, Google Scholar, Scilit, Europe PMC.

Copyright: This is an open access article distributed under the Creative Commons Attribution License which permits unrestricted use, distribution, and reproduction in any medium, provided the original work is properly cited.

Article

# Carbonization of Zr-Loaded Thiourea-Functionalized Styrene-Divinylbenzene Copolymers: An Easy Way to Synthesize Nano-ZrO<sub>2</sub>@C and Nano-(ZrC, ZrO<sub>2</sub>)@C Composites

Alejandro Martiz <sup>1,2</sup>, Zoltán Károly <sup>1</sup>, Laura Bereczki <sup>1</sup>, László Trif <sup>1</sup>, Attila Farkas <sup>3</sup>,  
Alfréd Menyhárd <sup>2</sup> and László Kótai <sup>1,4,\*</sup>

<sup>1</sup> Institute of Materials and Environmental Chemistry, Research Centre for Natural Sciences, Hungarian Academy of Sciences, Magyar Tudósok krt. 2., Budapest, H-1117, Hungary

<sup>2</sup> Budapest University of Technology and Economics, Department of Physical Chemistry and Materials Science, Műegyetem rakpart 3, Budapest, H-1111, Hungary

<sup>3</sup> Budapest University of Technology and Economics, Department of Organic Chemistry and Technology, Műegyetem rakpart 3, H-1111, Budapest, Hungary

<sup>4</sup> Deuton-X Ltd., Selmeci u. 89, H-2030, Érd, Hungary

\* Correspondence: kotai.laszlo@ttk.hu

**Abstract:** Thermal processing of Zr-loaded ion-exchangers is a facile route to synthesize (ZrO<sub>2</sub>, ZrC)@C composites. The chemical character of the functional groups in the cation exchanger is an essential factor in the composition and properties of the (ZrO<sub>2</sub>, ZrC)@C composites. In the present paper furnace and RF-thermal plasma processing of ZrOCl<sub>2</sub> loaded thiourea-functionalized styrene-divinylbenzene copolymer was investigated that led to various composites containing ZrO<sub>2</sub> and ZrC. Depending on the synthesis conditions, different ZrO<sub>2</sub>@C composites were formed between 1000 and 1400 °C in 2 h, whereas the composite containing ZrC was created at 1400 °C in 8 h. The ratio of ZrO<sub>2</sub>/ZrC, the prevailing ZrO<sub>2</sub> modifications, and the crystallite sizes strongly depend on the synthesis conditions. The ZrC-containing composites formed only at 1400 °C in 8 hours and by the plasma treatment of the ZrO<sub>2</sub>@C sample prepared in the furnace, resulting in 8 and 16% ZrC content, with 44 and 41 nm ZrC crystallite sizes, respectively. The ZrO<sub>2</sub>-containing composites (tetragonal, monoclinic, and cubic modifications with 65–88 nm ZrO<sub>2</sub> crystallite sizes and 15–43 m<sup>2</sup>/g BET surface areas, depending on the carbonization temperature) formed in a tube furnace between 1000 and 1400 °C in 2 h. The tube furnace-prepared sample formed at 1400 °C in 8 h contained ZrC, ZrO<sub>2</sub> modifications, and amorphous carbon, whereas the plasma-treated sample contained ZrC, ZrO<sub>2</sub> modifications, and graphite. All ZrO<sub>2</sub>@C composites had both amorphous carbon and graphite, and their ratio is temperature-dependent. The carbonaceous compounds of the prepared composites were characterized by Raman spectroscopy, with analysis of the G and D band intensities. XPS studies showed the surface oxidation of ZrC.

**Keywords:** zirconium carbide; zirconium dioxide; carbon matrix; graphite; RF plasma; carbonization; thiourea; styrene-divinylbenzene copolymer; Raman spectroscopy

## 1. Introduction

Radiolytically stable amorphous carbon and graphite composites containing ZrC and ZrO<sub>2</sub> have enormous strategic importance in the nuclear industry due to their advantages such as high mechanical strength, a high adsorption capacity towards fission products, and a large neutron absorption cross-section [1–4]. A recently developed new method to synthesize carbon composites containing metal oxides is based on the carbonization of ion exchangers with various functional groups (sulfonate, iminodiacetate) [5,6]. Some metals like titanium or zirconium form carbides at higher temperatures or during plasma treatment [7–9]. ZrC@C or (ZrC, ZrO<sub>2</sub>)@C composites were prepared from Zr-loaded sulfonate-, iminodiacetate-, or dimethylamine-functionalized ion-exchanger resins loaded with cationic, complexed, or anionic Zr-species, respectively. The functional

groups strongly influence carbide formation despite the loss of the functional groups below 500 °C due to the differences between the reactivity of the intermediates that formed from the various functionalized polymers[5,6,10,11]. The sulfonate-, iminodiacetate-, and dimethylamine-functionalized ion exchangers have S and O, N and O, and only N heteroatom-containing functional groups bound to zirconium. Therefore, in the present paper, we tested an ion exchanger with an S, N-type active group—thiourea linked through a methylene group to the styrene-divinylbenzene skeleton - as a precursor of carbon composites containing ZrO<sub>2</sub> and (ZrO<sub>2</sub>, ZrC). We studied the formation of (nano-ZrC, nano-ZrO<sub>2</sub>)@C composites in a high-temperature tube furnace from Zr-loaded thiourea-functionalized resin. The distribution of zirconium in the functional groups is homogeneous at the atomic level, which promises to enhance the uniformity of the distribution of ZrO<sub>2</sub> and ZrC in the carbon matrix. The properties and composition of nano-(ZrC<sub>x</sub>, ZrO<sub>2</sub>)@C composites prepared in a tube furnace at 1400 °C for 8 h and the samples made by post RF plasma treatment in a He atmosphere were characterized in detail.

## 2. Materials and Methods

The thiourea-functionalized resin (Resinex CH-80-L) and other chemicals (HCl, zirconyl chloride, and other analytical reagents) were supplied by Deuton-X Ltd, Hungary.

### Experimental

#### *Preparation of Zr-loaded samples*

The thiourea-functionalized styrene-divinylbenzene copolymer containing 2% DVB was soaked in 3 M aq. HCl for 24 hours, the swelled beads were transferred into a long (20 cm) glass column. The Zr loading process was performed with a zirconyl chloride solution containing 0.5 wt.% Zr in 3 M HCl [5]. The Zr-loaded sample was dried at 90 and 110 °C in air for 3 and 2 h, respectively. The dry beads were left to cool in a sealed desiccator containing freshly prepared calcium oxide.

#### *Elemental analysis*

The CHNS analysis of the Zr-loaded sample was performed using a Carlo Erba 1106 (Cormaredo, Italy) instrument. The sample was dried in a vacuum oven at 140 °C for 19 h, and the dry sample was stored in a glass vial filled with nitrogen and tightly capped. Zr content was measured with the ICP-OES method [12].

#### *Carbonization experiments*

The Zr-loaded sample was ground in a planetary ball mill (225 rpm, 30 min), reducing the particle size below 63 μm. In each experiment, 1.5 g of the sample was placed into a quartz boat. Pyrolysis (carbonization) was performed in a tubular furnace supplied with an alumina tube under an argon atmosphere at 1000, 1200, and 1400 °C for 2 h and 1400 °C for 8 h. The heating rate was 15 °C min<sup>-1</sup> and the volume flow rate of the argon gas (1.5 L·min<sup>-1</sup>) was kept constant during the experiments.

#### *RF thermal plasma processing*

Because of the 20.3 wt.% of residual water content in the Zr-loaded resins (Table S1) and the shortness of residence time of the resin beads in the plasma plume, direct carbonization cannot produce carbonized samples. Therefore, the sample carbonized preliminary at 1000 °C for 2 h, which contained only ZrO<sub>2</sub> and elemental carbon, was subjected to in-flight RF thermal plasma treatment in a helium or hydrogen atmosphere. The experimental setup [13-15] consisted of a reactor chamber, which was supplied with an RF inductively coupled plasma torch mounted on the top (type PL-35, TEKNA Ltd, Sherbrooke, Canada), an RF generator (LEPEL, Waukesha, USA, with a maximum power of 30 kW at 4–5 MHz), a cyclone, a filter unit, and a vacuum pump [5]. Each sample was delivered into the plasma as described in Martiz et al. [5] with the use of a Praxair feeder (He as a carrier gas, with a flow rate of 5 L·min<sup>-1</sup>) at a feeding rate of 3 g·min<sup>-1</sup>. The location of the feeding probe was coaxial in the middle of the induction coil, and the plasma gas and the sheath gas were an 11:6 and a 35:5 L·min<sup>-1</sup> mixture of Ar and He, respectively. The main operating conditions (70 kPa and 25 kW of power) for each test were adapted from [15].

#### *Specific surface area measurements*

The surface area of the carbonized samples was determined with the Brunauer-Emmett-Teller (BET) equation based on nitrogen adsorption data (collected at  $-196\text{ }^{\circ}\text{C}$ , Autosorb 1C, Quantachrome, Boynton Beach, USA). The samples were evacuated before the measurements at  $100\text{ }^{\circ}\text{C}$  for 24 h.

#### *Transmission Electron Microscopy*

Transmission Electron Microscopy (TEM) was carried out with a 200 keV (Talos Thermo Scientific, Waltham, USA) electron microscope. The carbonized grains were crushed in EtOH and deposited onto the surface of Cu grids covered by Lacey carbon [5]. Selected-area electron diffraction patterns (SAED) were obtained. The current in TEM mode was  $\sim 600\text{ pA}$ , and the SAED patterns were acquired using a camera length of 520 mm. [13].

#### *Thermal studies*

Thermogravimetric analysis, differential scanning calorimetry, and mass spectrometric evolved gas analysis were performed simultaneously with the use of a SETARAM Labsys Evo (Lyon, France) and a Pfeiffer Vacuum OmniStar (Asslar, Germany) instruments under a He atmosphere (heating rate  $20\text{ }^{\circ}\text{C}/\text{min}$ ,  $25\text{--}1000\text{ }^{\circ}\text{C}$ ). The details of the thermal analysis were given in [5,6].

#### *Powder X-ray Diffraction*

The powder XRD patterns were acquired with the use of a Bragg-Brentano parafocusing goniometer (Philips, Amsterdam, Netherland) Cu weighted  $K\alpha$  radiation,  $1.5406/1.5444\text{ \AA}$  in the  $2\theta$  range of  $4\text{--}70^{\circ}$  (step size  $0.02^{\circ}$ , 1 s interval time). Despite the known unit cell dimensions of the ZrC and  $\text{ZrO}_2$  phases, the composition of phases has to be considered an estimate rather than accurate due to the amorphous carbon content and problems in determining the background. The other details of the XRD analysis were given in [5,6].

#### *Vibrational spectroscopy*

The IR and far-IR spectra were collected from 16 scans and acquired with a resolution of  $4\text{ cm}^{-1}$  on a Bruker Alpha FT-IR (Bruker, Ettingen, Germany) and a Biorad-Digilab FTS-30 instrument (Biorad, Budapest, Hungary), respectively, in Attenuated Total Reflectance (ATR) mode [16-18]. The Raman spectra were recorded with the use of a Horiba Jobin-Yvon LabRAM micro-spectrometer (Horiba France SAS, Longjumeau, France, external Nd-YAG laser, 532 nm) focusing the laser beam on an objective (20X, numerical aperture = 0.4) with the use of D0.3 or D0.6 optical filters to reduce the intensity of the laser beam to avoid degradation. A grating monochromator ( $1800\text{ mm}^{-1}$  for light dispersion) and  $1000\text{ }\mu\text{m}$  of the confocal hole were attached. The wavenumber scanning resolution was  $3\text{ cm}^{-1}$ , and the accumulation time was 90–120 s per point for the spectral range ( $3400\text{--}200\text{ cm}^{-1}$ ).

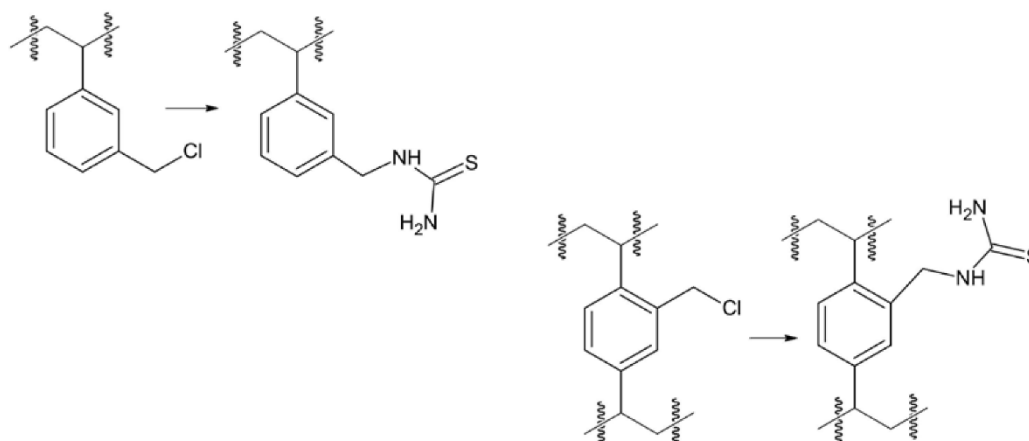
#### *X-ray photoelectron spectroscopy*

The XPS (X-ray photoelectron) spectra were recorded with a Kratos XSAM 800 instrument (Manchester, UK) in fixed analyzer transmission mode. Pass energy of 40 eV, Mg  $K_{\alpha 1,2}$  ( $1253.6\text{ eV}$ ) excitation, and  $< 1\cdot 10^{-7}\text{ Pa}$  chamber pressure were applied. Survey spectra were recorded in the 100–1300 eV kinetic energy range. The high-resolution spectra of the main PE lines of Zr, O, and C were recorded with 0.1 eV steps and a dwell time of 1 s. The quantitative analysis after removing the Shirley background was performed with the XPS MultiQuant program using experimentally determined cross-section data and asymmetry parameters [19,20].

### **3. Results**

#### *Preparation and properties of the Zr-loaded thiourea-functionalized resin*

The styrene-divinylbenzene skeleton is chloromethylated only in meta-position with chloromethyl methyl ether. Thus the consecutive coupling with thiourea results in only the meta-substituted thiourea-functionalized resin. The divinylbenzene is present only in 2%. Therefore, the functionalization of DVB units has marginal importance in the properties of the ion-exchange resin (Scheme 1).



**Scheme 1.** The structural units of the thiourea-functionalized crosslinked styrene-divinylbenzene copolymers.

The zirconium(IV) ion hydrolyzes and polymerizes in aqueous solutions even at low pH values, and the zirconyl ion ( $\text{ZrO}^{2+}$ ) is the only form of zirconium(IV) species in aqueous solutions at  $\text{pH} > 0$ . Zirconium (IV) ions form only in  $>12$  M HCl solutions and at a very low zirconium concentration (0.0001 M) [21]. Although the zirconyl chloride octahydrate is a tetramer ( $[\text{Zr}_4(\text{OH})_8(\text{H}_2\text{O})_{16}\text{Cl}_8]$ ) in the solid state, the zirconyl ion is the dominant chemical form in its aqueous solutions. Therefore, we used a 0.055 M zirconyl chloride solution in 3 M HCl in the Zr-loading of the thiourea-functionalized resin because the other available zirconium salts, zirconium sulfate ( $\text{H}_2[\text{ZrO}(\text{SO}_4)_2]$ ) and nitrate ( $\text{ZrO}(\text{NO}_3)_2$ ) contain the zirconium in anionic or neutral species in their solution, respectively [21-23].

The CHNS and Zr content of the Zr-loaded sample showed (ESI Table S1) that the amount of thiourea groups is  $\sim 0.4/\text{ring}$ , thus, not all the rings are functionalized. The S and Zr content shows that only 17% of the functional groups are loaded with zirconyl ions. The swelling water content is  $\sim 20\%$ . No chloride ion was detected in the sample, thus, the deprotonated thiourea group is the anion. The weak N-donor properties of thiourea suggest sulfur ligation [24]. The IR spectra (fingerprint region) of the unloaded and Zr-loaded samples were very similar because only a part of the thiourea groups was in complex (ESI Figure S1). The scissoring deformation mode of the swelling water gives intense broadband at  $1634\text{ cm}^{-1}$  with a shoulder ( $\text{NH}_2$  deformation band at  $1604\text{ cm}^{-1}$ ) (Figure 1) [25]. In contrast, the scissoring water deformation and OH stretching bands disappear in the IR spectrum of the dried Zr-loaded sample (Figure 1, ESI Figure S1). It shows the lack of coordinated water in the Zr coordination environment.

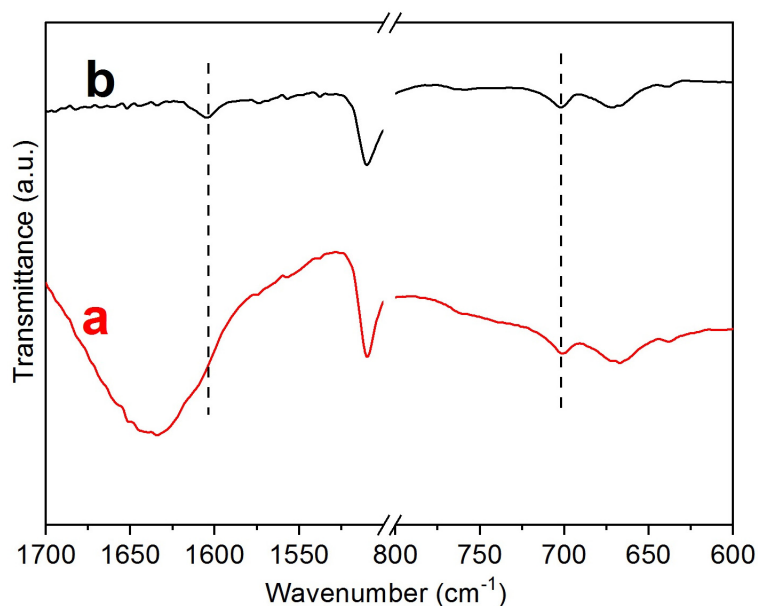


**Figure 1.** IR spectra of the raw (a) and Zr-loaded thiourea-supported styrene-divinylbenzene (b) copolymers in the 800–600 and 1700–1500  $\text{cm}^{-1}$  ranges.

The band at 1000–870  $\text{cm}^{-1}$  is characteristic of the zirconyl ion (or other product containing a condensed Zr-O bond) [23,26–28], but it coincides with different vibrational modes of the skeleton. Yuchi et al. stated that Zr-saturated resins with various functional groups contain R-Zr(OH)<sub>2</sub> species, but the IR spectrum of the dry resin does not contain OH bands at all, so these functional groups transform into Zr=O or condensed Zr-O bond species during drying [28,29]. The peak observed at 1420  $\text{cm}^{-1}$  in the spectra of free thiourea-functionalized and Zr-loaded resins may be attributed to the stretching vibrations of C=S groups, while the peak with a maximum at 1110  $\text{cm}^{-1}$  can be attributed to the rocking mode of the NH<sub>2</sub> group [25].

#### *Thermal studies of the Zr-loaded thiourea-functionalized STY-DVB resin*

The carbonization of the Zr-loaded thiourea-functionalized STY-DVB resin under inert conditions (ESI Figure S2) was a long decomposition process, which consists of parts belonging to the degradation of the thiourea functional group (~200–250 °C) together with the partial degradation of the polymer skeleton, followed by the multi-step depolymerization of the polymer skeleton (350–500 °C, Figure 2). The functional group loss process proceeds with the formation of various fragments ( $m/z=26, 27, 44, 58, 59, 60,$  and  $75$  corresponding to  $\text{CN}^+, \text{HCN}^+ (\text{HNC}^+), \text{CS}^+ (\text{CO}_2^+, \text{N}_2\text{O}^+)$   $\text{CNS}^+, \text{HSCN}^+$  or  $\text{HNCS}^+, \text{H}_2\text{NCS}^+$  or  $\text{H}_2\text{NCSH}^+$ , respectively) from the  $\text{CH}_2\text{HNCSNH}_2^+$  parent ion (Figure 2a), together with hydrocarbon fragments from the degradation of the aromatic ring ( $m/z=64$  (Figure 2b)), which shows that the functional groups are eliminated with a partial decomposition of the polymer skeleton between 250 and 500 °C (the  $m/z=64$  signal belongs to the  $\text{C}_5\text{H}_4^+$  fragment ion from aromatic ring fragmentation) [30].

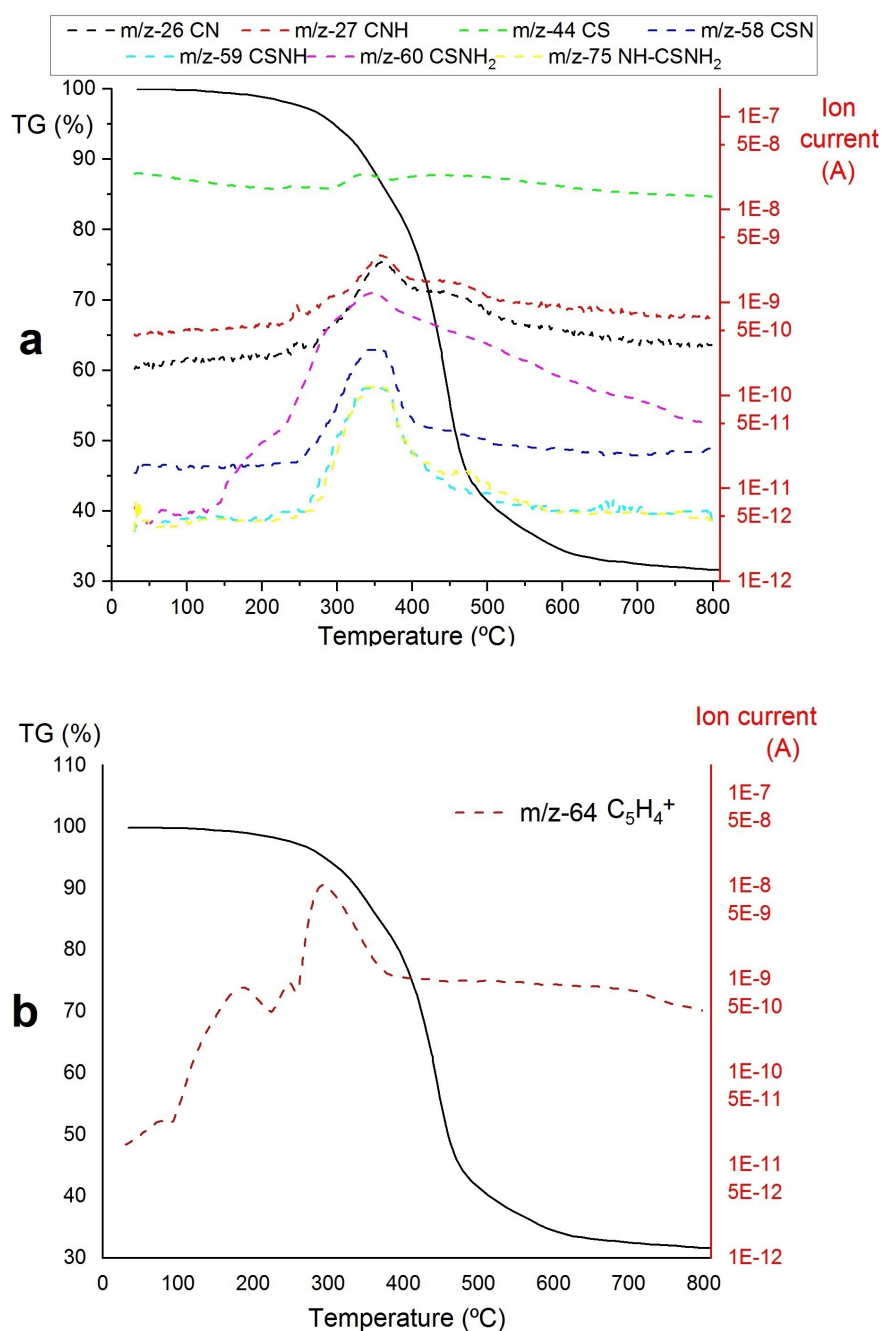


**Figure 2.** TG-MS plots of Zr-loaded thiourea-supported styrene-divinylbenzene copolymer carbonization. Fragments of functional group (a), hydrocarbon fragments from the decomposition of aromatic rings (b).

The expected decomposition product at  $m/z=44$  is the  $CS^+$  fragment, but  $CO_2^+$  and  $N_2O^+$  can also signal at  $m/z=44$ . To distinguish these species, we followed the evolution of the  $m/z=28$  ( $CO^+$ ,  $N_2^+$ ) and  $m/z=32$  ( $S^+$ ) fragments because the  $m/z=28$  ( $CO^+$  or  $N_2^+$ ) fragments may be formed only from  $CO_2^+$  or  $N_2O^+$ , respectively, whereas  $m/z=32$  ( $S^+$ ) fragment only from  $CS$  parent ions. The shape of the  $CO^+/N_2^+$  curve ( $m/z=28$ ) does not entirely coincide with the shape of the  $CO_2^+/N_2O^+/CS^+$  curve, thus the  $m/z=44$  peak consists of at least two ion signals, one of which generates an  $m/z=28$  fragment ion and at least one other which does not cause an  $m/z=28$  fragment ion (Figure 3). Evaluation of the  $m/z=32$  curve did not give valuable information due to the high reactivity of sulfur vapor and possible  $O_2$  traces. The evolution of water was followed by monitoring the peaks at  $m/z=18$  ( $H_2O^+$ ) and  $m/z=17$  ( $OH^+$ ). The  $m/z=16$  ( $O^+$  and  $NH_2^+$ ) peak intensities were compared with the peak intensities of  $m/z=15$

( $\text{NH}^+$ ,  $\text{CH}_3^+$ ) and  $m/z=14$  ( $\text{N}^+$  and  $\text{CH}_2^+$ ) fragment ions, which showed that the  $m/z=15$  and 14 intensity ratio is changed with increase the temperature. It may be attributed to the  $\text{CH}_3$  ion formation with H abstraction during the high-temperature polymer skeleton degradation. Accordingly, the  $m/z=15$  and 14 peaks contain more N and NH fragments around 350 °C, whereas the contribution of  $\text{CH}_3$  and  $\text{CH}_2$  fragments at 450-500 °C is higher than at ~350 °C, respectively (Figure 3).

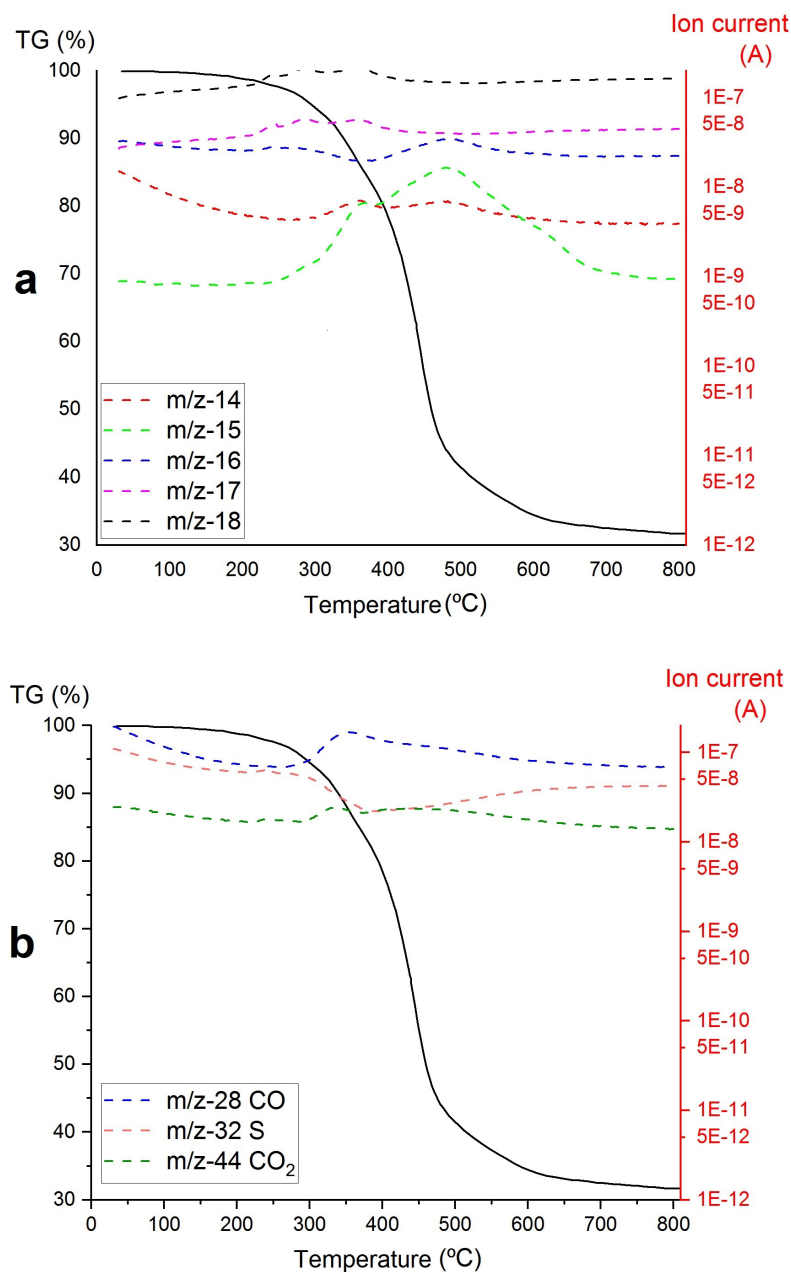


**Figure 3.** TG-MS plots of Zr-loaded thiourea-supported styrene-divinylbenzene copolymer carbonization. Evolution of water ( $m/z=18$  ( $\text{OH}_2^+$ ) and 17 ( $\text{OH}^+$ )) and  $m/z=15$  ( $\text{NH}^+$ ,  $\text{CH}_3^+$ ) and  $m/z=14$  ( $\text{N}^+$  and  $\text{CH}_2^+$ ) fragment ions (a).  $m/z=44$  parent ions and their fragments (b).

The decomposition process may be described with the following steps:

- The decomposition of the Zr-loaded thiourea groups with partial depolymerization/degradation of the rings attached to the Zr-loaded thiourea functions
- The degradation of unfunctionalized thiourea groups with partial depolymerization and degradation of the rings attached to the unloaded thiourea groups

- C) complete depolymerization/degradation of the residual polymer matrix at ~ 500 °C [5,6]. The other minor effects are the decomposition of residual materials, including the N and S containing carbonaceous materials formed in the previous decomposition steps.

Polymer degradation proceeded with the formation of Ph-CHCH<sup>+</sup> (m/z=103), PhCH<sup>+</sup> (m/z=91), C<sub>6</sub>H<sub>x</sub><sup>+</sup> (x=3,4,5, m/z=63,64,65), and DVB fragments (m/z=130,129,128) (ESI Fig. 3). The low DVB content does not help the formation of large amounts of solid carbonaceous products [31], but metal loading generally increases the formation of solid products [32-34]. The amount of solid residue was >30%, with ~2.8% Zr content and ~20% water content. Thus, the solid carbonaceous products have ~9-10 C/Zr atomic ratio values. S and N might also be incorporated into the carbonaceous residue in the same amount.

The decomposition process is completed at around 800 °C. Therefore, the lowest carbonization temperature was selected to be 1000 °C.

#### *The preparation and properties of ZrO<sub>2</sub>@C composites*

The carbonization reactions were investigated first at 1000, 1200, and 1400 °C for 2 h in a tube furnace. To assess the impact of reaction time, the holding time was prolonged up to 8 h at 1400 °C. ZrC formed only at 1400 °C in 8 h, whereas ZrO<sub>2</sub> was created at all three studied temperatures. Tetragonal and monoclinic ZrO<sub>2</sub> were detected at 1000 °C, embedded in graphite and amorphous carbon. Treatment temperature and reaction time significantly affected the ratio of tetragonal and monoclinic ZrO<sub>2</sub> [35], which had values of 0.375, 0.38, 0.83, and 1.2 for tests conducted at 1000, 1200, and 1400 °C for two hours and at 1400 °C for eight hours, respectively. Cubic ZrO<sub>2</sub> was formed only at 1400 °C carbonization temperature, and its amount also increased with increasing treatment time. Amorphous carbon content decreases from ~48% (1000 °C for 2 h) to 22% (1400 °C for 2 h), and increasing the reaction time to 8 h at 1400 °C causes a further decrease (~10%) (Table 1).

**Table 1.** Composition and properties of (ZrC, ZrO<sub>2</sub>)@C composites prepared from the Zr-loaded thiourea functionalized styrene-divinylbenzene copolymer.

Sample	Carbon content [wt%]		ZrO <sub>2</sub> content and size [wt%, nm]			ZrC content and size [wt%, nm]
	Graphite	Amorphous carbon	Tetra	Mono	Cubic	
R_1000C-2h	30	~48	6 (85)	16 (80)		
R_1200C-2h	26	~34	11 (88)	29 (74)		
R_1400C-2h	38	~22	15(76)	18(71)	7(61)	
R_1400C-8h	32	~10	18(71)	15(66)	15(52)	8(44)
R_1000C_2h_P_Ar-He	>35	--	27(65)	11(69)	11(53)	16(41)

The change in the BET surface areas shows the opposite tendency—they increase from 15 m<sup>2</sup>/g (1000 °C for 2 h) to 43 m<sup>2</sup>/g (1400 °C for 2 h) and 125 m<sup>2</sup>/g (1400 °C for 8 h) (Table 2).

**Table 2.** BET Surface Area of all the calcination products obtained in furnace and RF-Plasma reactor.

Sample	BET-specific surface area (m <sup>2</sup> /g)
R_1000C-2h	15
R_1200C-2h	27
R_1400C-2h	43
R_1400C-8h	115
R_1000C_2h_P_Ar-He	278

### *The preparation and properties of composites containing zirconium carbide*

Cubic ZrC ( $a = 4.6690 \text{ \AA}$ , Fm3m) appeared with a crystallite size of  $\sim 44 \text{ nm}$  at  $1400 \text{ }^\circ\text{C}$  in 8 h. The RF plasma treatment of the sample prepared at  $1000 \text{ }^\circ\text{C}$  in 2 h (30% graphite, 48% amorphous carbon, 6% and 16% tetragonal and monoclinic  $\text{ZrO}_2$ , respectively), promoted the formation of ZrC (16%), which was the highest among all test conditions. The composite's average crystallite size and BET surface area were  $41 \text{ nm}$  and  $278 \text{ m}^2/\text{g}$ , respectively. The amorphous carbon content completely disappeared on RF plasma treatment in He [5], and all three  $\text{ZrO}_2$  modifications were present (tetragonal, monoclinic, and cubic, in 27%, 11%, and 11%, and with an average crystallite size of 65, 69, and 53 nm, respectively).

The TEM study on the samples containing ZrC prepared at  $1400 \text{ }^\circ\text{C}$  for 8 h and by RF plasma treatment can be seen in Figures 4 and 5. These samples exhibited similarities in their composition, e.g., they had both monoclinic and tetragonal  $\text{ZrO}_2$  phases, but there was no evidence of the ZrC cubic phase.

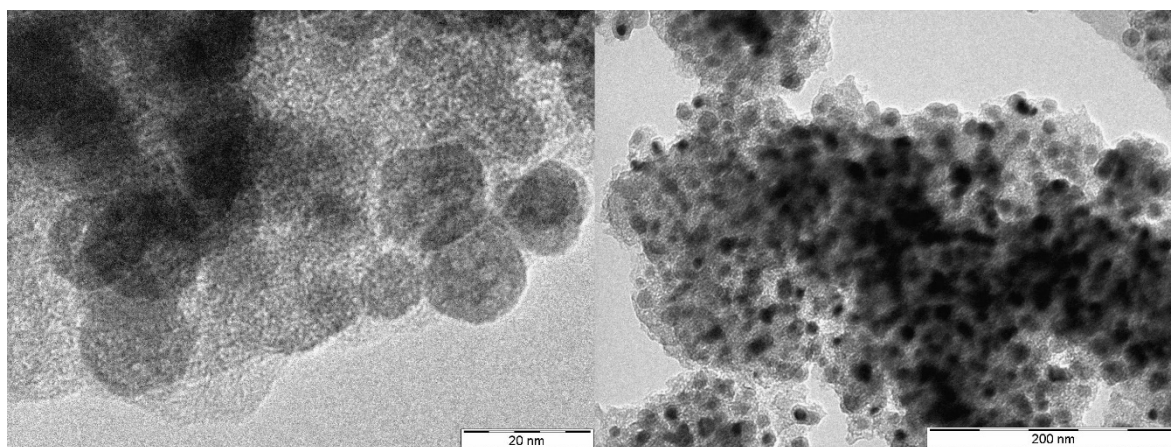


**Figure 4.** TEM images of the  $(\text{ZrC}, \text{ZrO}_2)@\text{C}$  composites prepared at  $1400 \text{ }^\circ\text{C}$  in 8 h from the Zr-loaded thiourea-functionalized styrene-divinylbenzene copolymer.

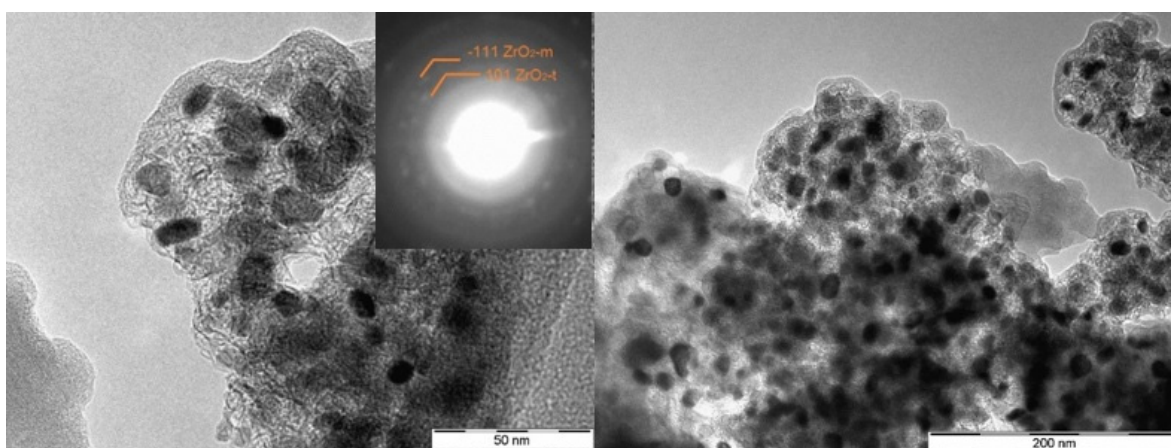


**Figure 5.** TEM images of the  $(\text{ZrC}, \text{ZrO}_2)@\text{C}$  composites prepared by plasma treatment of  $\text{ZrO}_2@\text{C}$  composite prepared at  $1000 \text{ }^\circ\text{C}$  in 2 h from the Zr-loaded thiourea functionalized styrene-divinylbenzene copolymer (Miller indices 111 and 101 are shown for monoclinic and tetragonal  $\text{ZrO}_2$ , respectively).

### *Raman studies on $\text{ZrO}_2@\text{C}$ and $(\text{ZrC}, \text{ZrO}_2)@\text{C}$ composites*

Raman spectroscopy gives information about the amount of carbonaceous phases, such as amorphous carbon, graphite, or distorted graphite structures, and the graphitization process [36-39]. The highly ordered monocrystalline graphite with an ideal graphite lattice gives two first-order Raman shifts. These are the harmonic transverse optical mode neighboring the zone boundary K

point, G ( $E_{2g}$ ), and the degraded optical mode at the Brillouin zone,  $G_1$  (2D), at  $\sim 1580$  and  $\sim 2687$   $\text{cm}^{-1}$ , respectively [40,41]. The disordered graphitic lattice possesses the band  $D_1$  (D) ( $A_{1g}$ , phonon of the longitudinal in-plane optical branch) and  $D_2$  ( $D'$ ) ( $E_{2g}$ , in-plane acoustic branch neighboring the K point), due to the graphene layer surfaces and edges, at around  $1350$  and  $1620$   $\text{cm}^{-1}$ , respectively [5,42,43]. The amorphous carbon  $D_3$  band ( $D''$ ) is located at  $1500$   $\text{cm}^{-1}$ , whereas the  $D_4$  ( $D^*$ ) band at  $1200$   $\text{cm}^{-1}$  consists of mixed modes including a graphite lattice disordered mode ( $A_{1g}$ ) and ionic impurity or polyene modes [36,39]. The Raman spectra of carbonaceous materials include weak combination ( $D + D''$ ) and harmonic overtone ( $2D'$ ) modes as well [43-45]. The Raman spectra of the ZrC-containing composites prepared from Zr-loaded thiourea-supported STY-DVB resin between  $1000$  and  $1400$   $^{\circ}\text{C}$  are given in Table 2 and ESI Figure 4.

The intensity ratio of the peaks belonging to amorphous/graphitic components ( $D''/(D+G)$ ) drops steadily as the reaction temperature increases, suggesting increasing graphitization. The same result was also observed in the Raman spectrum of the plasma-treated sample. Due to the creation of more crystalline phases, the D and G bands become sharp. The intensities of the  $D^*$  bands decrease drastically above  $1200$   $^{\circ}\text{C}$ , illustrating the decomposition of the organic polyenes. The D bands' stability on changing the temperature and carbonization time demonstrates low-level degradation of the surface graphene layers. The  $I_{D}/I_G$  ratio, proportional to the thickness of the monolayer carbon sheets, varies only a little and randomly with increasing reaction temperature and time. It shows that Zr atoms were not substantially absorbed into the carbon network [46]. Graphite formation may also be attributed to the catalytic effect of ZrC and the increasing temperature above  $1400$   $^{\circ}\text{C}$  [47]. The more ZrC is formed, the more graphite appears.

In the case of the furnace-treated samples, the increased reaction time and temperature resulted in soft improvements in the graphitization process. The amorphous carbon/graphite ratio decreases with increasing temperature. The Raman spectrum of the plasma-treated sample illustrates the complete disappearance of the  $D^*$  bands and the thermal decomposition of polyenes and their transformation into the superficial graphene layers.

XPS studies of the carbonized samples were performed to follow the changes in the state of carbon in the samples. The carbon 1s spectra were fitted using asymmetric peak shape AS(40, 0.6), usually used for graphite samples, on the carbonized samples (Figure 6). The spectra contain satellites and confirm the aromatic nature of the carbon phases. In the spectra of the plasma-treated samples, oxidized carbon species can be seen, which were not present in the XPS C1 spectra of the furnace heat-treated samples. No Zr-compounds were detected at the surface layer, which suggest that an outer carbon-containing layer was formed from the evaporated volatile hydrocarbon degradation products during the pyrolysis process.

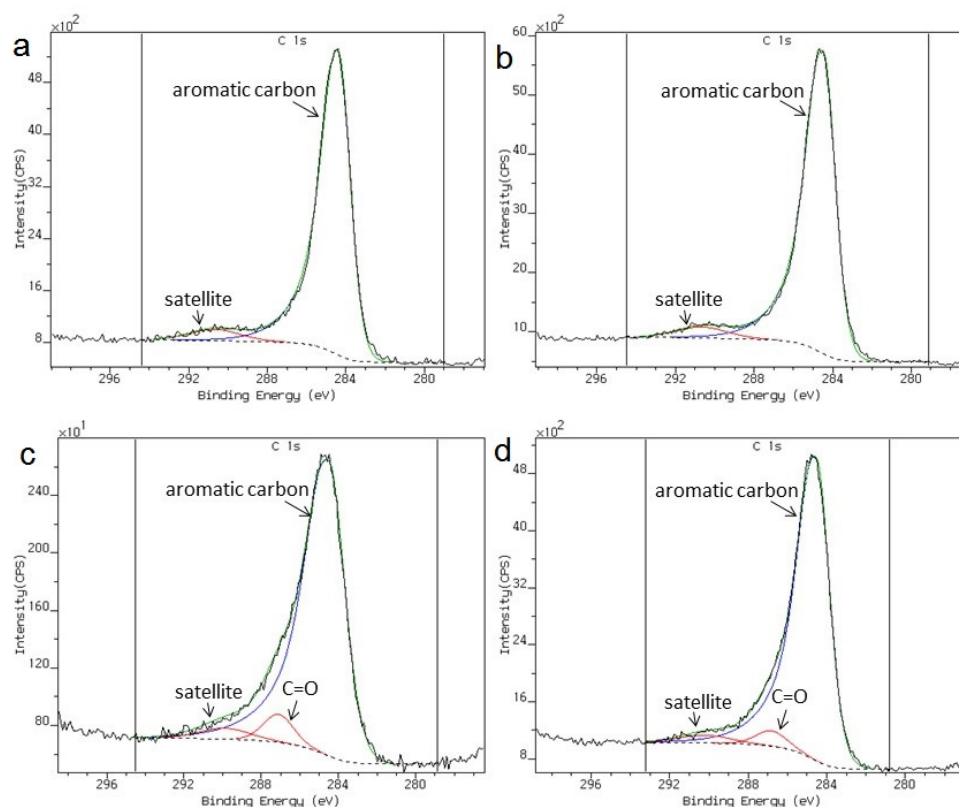


**Figure 6.** C<sub>1s</sub> XPS spectra of the carbonized Zr-loaded thiourea-functionalized styrene-divinylbenzene copolymer samples (a) 1400 °C for 2 h; (b) 1400 °C for 8 h; (c) Plasma treated in H<sub>2</sub> atmosphere; (d) Plasma treated in He atmosphere.

*Comparison of the ZrC containing composites prepared from various functionalized styrene-divinylbenzene based cation exchangers*

The ZrC-containing composites have high importance in the nuclear industry. The properties of the carbon-based composites containing ZrC and ZrO<sub>2</sub>, prepared from various cation exchangers, are summarized in Table 3.

**Table 3.** Carbon-based composites containing ZrC and ZrO<sub>2</sub>, prepared by the carbonization of various functionalized styrene-divinylbenzene polymer based cation exchangers.

Functional group	Conditions	ZrO <sub>2</sub> content and crystallite size	ZrC content and crystallite size	Ref.
-SO <sub>3</sub> H, ZrOCl <sub>2</sub> loaded	1400 °C, 8 h, 2% DVB	7% tetragonal and 11% monoclinic, each size was 32 nm	No ZrC formation	[5]
	1400 °C, 8 h, 8% DVB	<5% tetragonal and <5% monoclinic, 20 and 27 nm, respectively	No ZrC formation	[5]
	RF Plasma, He	16% tetragonal, 13% monoclinic, <5% cubic, 20, 27 and 27 nm, respectively	11% ZrC, 23 nm >55% graphite content	[5]
	RF Plasma, H <sub>2</sub>	17% tetragonal, 10% monoclinic, <5% cubic, 18, 27, and 22 nm, respectively	13% ZrC, 21 nm >55% graphite content	[5]

-CH <sub>2</sub> -NHC(S)NH <sub>2</sub>	1400 °C, 8 h, 2% DVB	18% tetragonal, 15% monoclinic, 15% cubic, 71, 66, and 52 nm, respectively	8% ZrC content, 44 nm (32 and 10% graphite and amorphous C content)	
	RF plasma, He	27% tetragonal, 15% monoclinic, 11% cubic, 65, 69, and 53 nm, respectively	16% ZrC content, 41 nm (only graphite is present as carbonaceous phase)	
-CH <sub>2</sub> - N(CH <sub>2</sub> COOH) <sub>2</sub> , ZrOCl <sub>2</sub> loaded	1200 °C, 2 h	15% tetragonal, 11 nm	75% ZrC, 10 nm (no graphite and 10% amorphous C content)	[6]
-CH <sub>2</sub> - N(CH <sub>2</sub> COOH) <sub>2</sub> , ZrOCl <sub>2</sub> loaded	1400 °C, 8 h	5% tetragonal/monoclinic=1.92, 26 nm	85% ZrC, 14 nm (no graphite and 10% amorphous C content)	[6]
-CH <sub>2</sub> - N(CH <sub>2</sub> COOH) <sub>2</sub> , Zr- sulphate loaded	1400 °C, 8 h	5% monoclinic/cubic=1.05, 31 nm	50% ZrC, 56 nm (no graphite and 45% amorphous C content)	[6]
-CH <sub>2</sub> - N(CH <sub>2</sub> COOH) <sub>2</sub> , Zr- nitrate loaded	1400 °C, 8 h	No ZrO <sub>2</sub>	95% ZrC, 18 nm (5% amorphous C content)	[6]
-CH <sub>2</sub> - N(CH <sub>2</sub> COOH) <sub>2</sub> , Zr- nitrate loaded	RF plasma, He	No ZrO <sub>2</sub>	95% ZrC, 62 nm (5% graphite)	[6]
-CH <sub>2</sub> - N(CH <sub>2</sub> COOH) <sub>2</sub> , Zr- nitrate-loaded	RF plasma, H <sub>2</sub>	No ZrO <sub>2</sub>	90% ZrC, 35 nm (10% graphite)	[6]

As shown in Table 3, the ZrC content and crystallite size strongly depend on the functional groups of the precursor ion exchanger and the carbonization conditions. Thus, the method (tube furnace and plasma treatment carbonization) can result in different compositions with various ZrO<sub>2</sub>/ZrC ratios (ESI Figure S5). Different ratios of each ZrO<sub>2</sub> modification were found and had various crystallite sizes. The functional groups of the anion exchangers were similarly crucial in the distribution of ZrC and ZrO<sub>2</sub>, including the modifications of ZrO<sub>2</sub> [48].

#### 4. Conclusion

Various composites with different ZrO<sub>2</sub> and ZrC content with varying ratios of each ZrO<sub>2</sub> modification were prepared from a ZrOCl<sub>2</sub>-loaded thiourea-functionalized styrene-divinylbenzene copolymer by carbonization in a tube furnace at 1400 °C as well as by in-flight thermal plasma treatment of the ZrO<sub>2</sub>@ sample made at 1000 °C in 2 h. The crystallite sizes of the ZrO<sub>2</sub> modifications and ZrC strongly depend on the synthesis conditions. The functional groups of the cation exchangers are an essential factor in preparing the (ZrO<sub>2</sub>, ZrX)@composites. The ZrC-containing composites were formed from the thiourea-functionalized and ZrOCl<sub>2</sub>-loaded samples at 1400 °C in 8 h and with in-flight plasma treatment in He with 8 and 16% ZrC, and 44 and 41 nm ZrC crystallite sizes, respectively. The BET surface area of the composite containing ZrC was 115 and 278 m<sup>2</sup>/g for the samples prepared in a tube furnace and by plasma processing, respectively. Carbide formation was time-dependent, with no detected ZrC at 1400 °C in 2 h. Lower temperatures (1000–1200 °C) and a short reaction time (2 h) resulted in only ZrO<sub>2</sub> modifications (tetragonal, monoclinic, and cubic) in various ratios and crystallite sizes (65–88 nm) and BET surface areas (15–43 m<sup>2</sup>/g).

**Supplementary Materials:** The following supporting information can be downloaded at the website of this paper posted on Preprints.org. ESI Table S1 Chemical analysis of Zr-loaded thiourea functionalized styrene-divinylbenzene copolymer (average of five measurements). ESI Table S2 Raman peak

positions (in  $\text{cm}^{-1}$ ) and intensities for  $(\text{ZrO}_2)\text{@C}$  and  $(\text{ZrO}_2,\text{ZrC})\text{@C}$  composite samples. ESI Figure 1 FT-IR spectra of the unloaded and Zr-loaded thiourea-functionalized styrene-divinylbenzene copolymer. ESI Figure 2 TG-DSC of the of the Zr-loaded thiourea-functionalized styrene-divinylbenzene copolymer under  $\text{N}_2$  atmosphere. ESI Figure 3 TG-MS of the Zr-loaded thiourea-functionalized styrene-divinylbenzene copolymer:  $\text{Ph-CHCH}^+$  ( $m/z=103$ ),  $\text{PhCH}^+$  ( $m/z=91$ ),  $\text{C}_6\text{H}_x^+$  ( $x=3,4,5$ ,  $m/z=63,64,65$ ) (a), and DVB fragments ( $m/z=130,129,128$ ) (b). ESI Figure 4 Raman spectra of the carbonized Zr-loaded thiourea-functionalized styrene-divinylbenzene copolymer at different temperatures and processes.  $1000\text{ }^\circ\text{C}$  for 2 hours (a),  $1200\text{ }^\circ\text{C}$  for 2 hours (b),  $1400\text{ }^\circ\text{C}$  for 2 hours (c),  $1400\text{ }^\circ\text{C}$  for 8 hours (d), plasma treated in He atmosphere (e). ESI Figure 5 XRD pattern of the samples produced by calcination of the Zr-loaded thiourea-functionalized sstyrene-divinylbenzene copolymer

**Author Contributions:** Conceptualization, LK; investigation, AM, ZK, LB, LT, AF, AM; writing—original draft preparation, LK, AM; writing—review and editing, ZK and LK; visualization, AM; supervision, KZ and LK; All authors have read and agreed to the published version of the manuscript.

**Conflicts of Interest:** The authors declare no conflict of interest.

## References

- [1] Liu, G.; Cheng, L.; Li, K.; Chen, Z.; Xiong, X.; Luan, X. Damage behavior of atomic oxygen on zirconium carbide coating modified carbon/carbon composite. *Ceram. Int.*, **2020**, 3:3324–31.
- [2] Pierson, HO. *Handbook of refractory carbides and nitrides: properties.; characteristics.; processing and applications*. 1<sup>st</sup> ed. Bergen: Noyes Publication, USA, 1997.
- [3] Scales, N.; Chen, J.; Aughterson, RD.; Karatchevtseva, I.; Stopic, A.; Lumpkin, GR.; et al. Porous ZrC-carbon microspheres as potential Insoluble target matrices for production of 188W/188Re. *J. Radioanal. Nucl. Chem.*, **2018**, 318(2), 835–47.
- [4] Scales, N.; Chen, J.; Hanley, T.L.; Riley, D.P.; Lumpkin, G.R.; Luca, V. Hierarchically porous carbon–zirconium carbide spheres as potentially reusable transmutation targets. *Microporous Mesoporous Mater.*, **2015**, 212:100–9.
- [5] Martiz, A.; Károly, Z.; Trif L.; Mohai, M.; Bereczki, L.; Németh, P.; Zsombor, M.; Menyhárd, A.; Pawar, R. P.; Kótai, L. Plasma-assisted preparation of nano-(ZrC.; ZrO<sub>2</sub>)@carbon composites from Zr-loaded sulfonated styrene–divinylbenzene copolymers. *J. Therm. Anal. Calorim.* **2022**, 147, 9353–9365.
- [6] Martiz, A.; Károly, Z.; Domján, A.; Mohai, M.; Bereczki, L.; Trif, L.; Farkas, A.; László, K.; Menyhárd, A.; Kótai, L. Nano-ZrO<sub>2</sub>@C.; nano-(ZrC.; ZrO<sub>2</sub>)@C and nano-ZrC@C composites prepared by plasma-assisted carbonization of Zr-loaded iminodiacetate-functionalized styrene-divinylbenzene copolymers. *Inorganics*, **2022**, 10 (6), 77.
- [7] Bai, L.; Yuan, F.; Fang, Z.; Wang, Q.; Ouyang, Y.; Jin, H.; He, J.; Liu, W.; Wang, Y. RF thermal plasma synthesis of ultrafine ZrB<sub>2</sub>-ZrC composite powders. *Nanomaterials*, **2020**, 10, 2497.
- [8] Peters, A.B.; Wang, C.; Zhang, D.; Hernandez, A.; Nagle, D.C.; Mueller, T.; Spicer, J.B. Reactive laser synthesis of ultra-high-temperature ceramics HfC, ZrC, TiC, HfN, ZrN and TiN for additive manufacturing. *Ceram. Int.*, **2023**, 49(7), 11204-11229.
- [9] Martiz, A.; Károly, Z.; Bódis, E.; Fazekas, P.; Mohai, M.; Bertóti, I.; Keszler, A.M. In-flight synthesis of nanosized ZrC particles from various precursors in RF thermal plasma. *Per. Polytech. Chem. Eng.*, **2021**, 65 (3). 331–342.
- [10] Saray, M. T.; Yurkiv, V.; Shahbazian-Yassar, R. In Situ Thermolysis of a Ni Salt on Amorphous Carbon and Graphene Oxide Substrates. *Adv. Funct. Mater.*, **2023**, 2213747.

- [11] Wei, Y.; FaZhan, X.; Xin, L.; Wei, H.; YongYue, Y.; DongChuang, W.; et al. Nickel and oxygen-containing functional groups co-decorated graphene-like shells as catalytic sites with excellent selective hydrogenation activity and robust stability. *Chem. Eng. J.*, **2023**, 452 (3).
- [12] Masoud, A.; Gholamhassan, A.; Mohammad, K. A. An on-line matrix separation and preconcentration procedure for ICP OES determination of Cd, Co, Cu, Mn and Pb traces in Zr and Zr–Nb alloys using a cation-exchange resin microcolumn. *J. Anal. Atom. Spectrom.*, **2021**, 36, 1074-1083.
- [13] Li, F.; Huang, X.; Zhang, G.J. Scalable foaming assisted synthesis of ZrC nanopowder by carbothermal reduction. *Ceram. Int.*, **2015**, 41:3335–8.
- [14] Fazekas, P.; Czégény, Z.; Mink, J.; Bódis, E.; Klébert, S.; Németh, C.; Keszler, A.M.; et al. Decomposition of poly(vinyl chloride) in inductively coupled radiofrequency thermal plasma. *Chem. Eng. J.*, **2016**, 302, 163–171.
- [15] Szépvölgyi, J.; Mohai, I.; Karoly, Z.; Gál, L. Synthesis of nanosized ceramic powders in a radiofrequency thermal plasma reactor. *J. Eur. Ceram.*, **2018**, 28(5), pp. 895–899.
- [16] Komarov, V.S.; Yatsevskaya, M.I.; Sycheva, O.A. Properties of activated carbon produced from spent ion-exchange resins. *Dokl. Akad. Nauk. BSSR*, **1985**, 29, 1010–1023.
- [17] Chinthaka, Silva, G.W.; Kercher, A.A.; Hunn, J.D.; Martin, R.C.; Jellison, G.E.; Meyer, H.M. Characterization of zirconium carbides using electron microscopy, optical anisotropy, Auger depth profiles, X-ray diffraction and electron density calculated by charge flipping method. *J. Solid State Chem.*, **2012**, 194.; 91–99.
- [18] Gusev, A.I. Structural stability boundaries for nonstoichiometric compounds. *Phys. Status Solidi A*. **1989**, 111, 443–450.
- [19] Mohai, M.; XPS MultiQuant: multimodel XPS quantification software. *Surf. Interface Anal.*, **2004**. 36(8).; pp. 828–832.
- [20] Mohai, M.; Bertóti, I. Calculation of overlayer thickness on curved surfaces based on XPS intensities. *Surf. Interface Anal.*, **2004**, 36(8).; pp. 805–808.
- [21] Wang, C.; Cheng, R.; Liao, L.; Duan, X. High-performance thin-film electronics based on inorganic nanostructures and composites. *Nano Today*, **2013**, 8.; 514–530.
- [22] Basumatary, S. Transesterification with heterogeneous catalyst in production of biodiesel: A review. *J. Chem. Pharm.*, **2013**, 5.; 1–7.
- [23] Fedorov, P.P.; Yarotskaya, E.G. Zirconium dioxide. Review. *Condens. Matter Interphases*, **2021**.; 23.; 169–187.
- [24] Loubalová, I.; Kopel, P. Coordination Compounds of Cu, Zn, and Ni with Dicarboxylic Acids and N Donor Ligands, and Their Biological Activity: A Review. *Molecules*, **2023**, 28(3).
- [25] Swaminathan, K.; Irving, H.M.N.H. Infra-red absorption spectra of complexes of thiourea. *J. Inorg. Nucl. Chem.*, V, **1964**, 26(7), 1291-1294.
- [26] Dunlap, C.J.; Mcneff, C.V.; Stoll, D.; Carr, P.W. Zirconia stationary phases for extreme separations. *Anal. Chem.*, **2001**, 73, 599A–607A.
- [27] Camps, M.; Chatzopoulos, M.; Camps, J.M.; Montheards, J.P. Chloromethylation of Polystyrenes and Styrene Copolymers. Applications. *JMS-Rev. Macromol. Chem. Phys.*, **1987**, 27, 505–557.
- [28] Yuchi, A.; Yoshida, N. Adsorption of tetravalent metal ions chelating resins containing iminodiacetic acid groups. *Bull. Chem. Soc. Jpn.*, **2000**, 73, 1841–1842.

- [29] Auer, B.M.; Skinner, J.L. IR and Raman spectra of liquid water: Theory and interpretation. *J. Chem. Phys.*, **2008**, 128, 224511.
- [30] Kotai, L.; Fodor, J.; Jakab, E.; Sajo, I. Szabo, P.; et al. A thermally induced low-temperature intramolecular redox reaction of bis(pyridine)silver(I) permanganate and its hemipyridine solvate. *Transit. Metal Chem.*, **2006**, 31, 30-34.
- [31] Lee, G.; Park, S. I.; Shin, H. Y.; Joh, H. I.; Kim, S. S.; & Lee, S. Simultaneous reactions of sulfonation and condensation for high-yield conversion of polystyrene into carbonaceous material. *J Ind Eng Chem*, **2023**, 122, 426-436.
- [32] Cheng, W.; Campolongo, M.J.; Tan, S.J.; Luo, D. Freestanding ultrathin nano-membranes via self-assembly. *Nano Today*, **2009**, 4, 482-493.
- [33] Kocsis, T.; May, Z.; Czégény, Z.; Sreedhar, B.; Pawar, R.P.; Kótai, L. Perspectives of magnetic and nanosized metal-containing amorphous carbon composite chemisorbents and catalysts. *Nano Studies*, **2016**, 14, 7-35.
- [34] Fazekas, P.; Czégény, Z.; Mink, J.; Bódis, E.; Klébert, S.; Németh, C.; Keszler, A.M.; Károly, Z.; Szépvölgyi, J. Decomposition of poly(vinyl chloride) in inductively coupled radiofrequency thermal plasma. *Chem. Eng. J.*, **2016**, 302, 163-171.
- [35] Wen, Y.; Zhou, C.; Yu, L.; Zhang, Q.; He, W.; & Liu, Q. Preparation of nanometer zirconia by hydrothermal method: Influence of temperature and mechanism. *Solid State Sci.*, **2023**, 107237.
- [36] Fitzgerald, J.J.; Weiss, R.A. Cation-Anion and Cation-Cation Interactions in Sulfonated Polystyrene Ionomers Spectroscopic Studies of the Effects of Solvents. *ACS Symp. Ser.*, **1986**, 302, 35-53.
- [37] El-Nahhall, I.M.; Zaggout, F.R.; Nassar, M.A.; El-Ashgar, N.M.; Maquet, J.; et al. Characterization and Applications of Immobilized Iminodiacetic Acid-Modified Silica. *J. Sol-Gel Sci. Technol.*, **2003**, 28, 255-265.
- [38] Jiang, J.; Renshaw, J.C.; Sarsfield, M.J.; Livens, FR.; Collison, D.; Charnock, J.M.; Eccles, H. Solution Chemistry of Uranyl Ion with Iminodiacetate and Oxydiacetate: A Combined NMR/EXAFS and Potentiometry/Calorimetry Study. *Inorg. Chem.*, **2003**, 42, 1233-1240.
- [39] Busca, G.; Lorenzelli, V. Infrared spectroscopic identification of species arising from reactive adsorption of carbon oxides on metal oxide surfaces. *Mater. Chem.*, **1982**, 7, 89-126.
- [40] Choi, J.G. The Effect of Surface Properties of Carbon Nanomaterials on the Molecular Adsorption of Organophosphate. *Graduate School of UNIST*, **2019**.
- [41] Komarov, V.S.; Yatsevskaya, M.I.; Sycheva, O.A. Properties of activated carbon produced from spent ion-exchange resins. *Dokl. Akad. Nauk. BSSR*, **1985**, 29, 1010-1023
- [42] Martiz, A.; Farkas, A.; Karoly, Z.; Franguelli, F.P.; Samaniego, S.K.; Menyhard, A.; Kotai, L. Raman studies on carbon-containing phases in nanosized-ZrO<sub>2</sub>/C and nanosized-(ZrC.; ZrO<sub>2</sub>)/C composites. *Nano Studies*, **2022**, 10, 21-22.
- [43] Lokshin, E.P.; Tareeva, O.A. Sorption of Zirconium from Nitrate and Sulfate Solutions. *Theor. Found. Chem. Eng.*, **2019**, 53, 688-692.
- [44] Clearfield, A. Structural aspects of zirconium chemistry. *Rev. Pure Appl. Chem.*, **1964**, 14, 91-108.
- [45] Fathy, M.; Moghn, T.A.; Awadallah, A.E.; El-Bellihi, A.H. Nano Composites of Polystyrene Divinyl Benzene Resin Based on Oxidized Multi-Walled Carbon Nanotubes. *Int. J. Modern Org. Chem.*, **2013**, 2, 67-80.

- [46] Shishlov, N.M.; Khurasan, S.L. Effect of ion interactions on the IR spectrum of benzenesulfonate ion. Restoration of sulfonate ion symmetry in sodium benzenesulfonate dimer. *J. Mol. Struct.*, **2016**, 1123, 360–366.
- [47] De, R.; Lee, H.; Das, B. Exploring the interactions in binary mixtures of polyelectrolytes: Influence of mixture composition.; concentration.; and temperature on counter-ion condensation. *J. Mol. Liq.*, **2018**, 251, 94–99.
- [48] Scales, N. Syntheses, structures and radionuclide extraction properties of porous ZrC-and Zr<sub>2</sub>SC-carbon composite sphere materials, *PhD Thesis*, University of Wollongong, **2018**.  
<https://ro.uow.edu.au/theses1/343>

**Disclaimer/Publisher's Note:** The statements, opinions and data contained in all publications are solely those of the individual author(s) and contributor(s) and not of MDPI and/or the editor(s). MDPI and/or the editor(s) disclaim responsibility for any injury to people or property resulting from any ideas, methods, instructions or products referred to in the content.